Electrochemistry Communications 114 (2020) 106714

Contents lists available at ScienceDirect

Electrochemistry Communications

journal homepage: www.elsevier.com/locate/elecom

Common mechanism for helical nanotube formation by anodic polymerization and by cathodic deposition using helical pores on silicon electrodes

Yuki Maeda[a], Takumi Yasuda[a], Kenta Matsuzaki[a], Yutaka Okazaki[b,c], Emilie Pouget[c], Reiko Oda[c], Atsushi Kitada[a], Kuniaki Murase[a], Guillaume Raffy[d], Dario M. Bassani[d], Kazuhiro Fukami[a,*]

[a] Department of Materials Science and Engineering, Kyoto University, Kyoto 606-8501, Japan
[b] Graduate School of Energy Science, Kyoto University, Kyoto 606-8501, Japan
[c] Institut de Chimie et Biologie des Membranes & des Nanoobjets (UMR5248 CBMN), CNRS – Université de Bordeaux – Bordeaux INP, 33607 Pessac, France
[d] Université de Bordeaux, CNRS, Bordeaux INP, ISM, UMR 5255, F-33405, Talence, France

ARTICLE INFO

Keywords:
Helical pore
Nanohelices
Conducting polymers
Metals
Tubes

ABSTRACT

We report that platinum-assisted chemical etching formed self-organized helical pores in silicon substrates can be utilized as platforms for the electrochemical production of nanohelices of conducting polymers (polypyrrole) and metals (gold). Surprisingly, the nanohelices thus created are tubes although the polymerization and deposition were carried out by anodic and cathodic reactions, respectively. Based on our results, we propose a common mechanism for the formation of tubular nanohelices by both anodic polymerization and cathodic deposition through the accumulation of reactants in microporous silicon which covers the wall surface of the helical pores.

1. Introduction

Helical nanometric structures are a form of chiral material which has found applications in enantioselective catalysis and circularly polarized light management [1–4]. A number of fabrication methods are known, either through top-down [5,6] or bottom-up methods [7]. For the latter, which gives access to sub-micron helices that are non-attainable with the top-down approach, the control of symmetry breaking is assured by molecular chirality. Meanwhile, the number of studies on the production and the use of chiral surfaces/helices by electrochemical techniques, although extremely promising for chiral recognition, synthesis and sensing [8–10] is still limited. The establishment of a general strategy for the production of nanohelices by an electrochemical technique would thus open a large panel of applications.

It has been reported that helical pores are spontaneously formed during platinum-assisted chemical etching (PacEtch) of silicon induced by the oxidation of silicon and reduction of H_2O_2 [11]. We have revealed that the emergence of helical pores originates from the symmetry breaking in the spatiotemporal pattern of H_2O_2 reduction, which is a spontaneous periodic reaction spatially coupled through the electrolyte solution [12]. The periodicity of the spatiotemporal pattern governs the periodicity in spiral of the helical pores. Therefore, one can control the dimensions of the helical pores by tuning the spatiotemporal patterns of H_2O_2 reduction.

Electrochemical techniques such as electrodeposition and electropolymerization are powerful tools to produce replicas of porous electrodes. Since silicon is a semiconductor, porous silicon can work as an electrode for electrochemical reactions and there are many reports of its use in producing microscopic structures of metals and conducting polymers [13–16]. Here, we report the filling of helical pores prepared by PacEtch of silicon achieved both by the electropolymerization of polypyrrole and the electrodeposition of gold. In earlier studies, it was reported that polypyrrole was deposited as tubes in non-helical (straight) porous silicon prepared by anodization of silicon in HF solutions without metallic catalysts, while metal was deposited as rods (without any cavities in the deposits) in such straight pores [13,14]. As a surprising result, the nanohelices both of polypyrrole and gold fabricated in the present study are made of tubes. Herein, we discuss a common mechanism of the electrochemical filling of the helical pores in silicon.

2. Experimental

Helical pores are formed in p-Si (100) with a resistivity of

* Corresponding author.
E-mail address: fukami.kazuhiro.2u@kyoto-u.ac.jp (K. Fukami).

https://doi.org/10.1016/j.elecom.2020.106714
Received 5 March 2020; Received in revised form 19 March 2020; Accepted 19 March 2020
Available online 22 March 2020

10–20 Ω cm. The p-Si substrate was subjected to ultrasonic cleansing in acetone and ultrapure water. The substrate was dipped into 5% HF to remove the native oxide layer, and then it was put in a platinum deposition bath composed of 1 mM H_2PtCl_6 + 150 mM HF aqueous solution to load the platinum nanocatalyst. Etchant was a mixture of 48% HF + 30% H_2O_2 (10:1 in volume). PacEtch was conducted for 10 min.

In the present study, we performed two different types of electrochemical filling, i.e., anodic electropolymerization and cathodic electrodeposition. Details for the reactions were published elsewhere [13,14]. Importantly, the conditions were as follows: electropolymerization of polypyrrole was conducted in an acetonitrile solution of 0.1 M pyrrole + 1.0 M tetrabutylammonium perchlorate under a constant current density of 127 μA cm^{-2}. Electrodeposition was carried out by cathodic polarization under a constant current density of –14 μA cm^{-2} in an aqueous solution of 0.01 M $HAuCl_4$ + 0.42 M $Na_2S_2O_3$ + 0.42 M Na_2SO_3. The silicon wafer was illuminated by a halogen lamp during gold deposition.

Transmission Electron Microscopy (TEM) was performed with a Philips EM 120 electron microscope operating at 120 kV, and the images were collected by 2 k × 2 k Gatan ssCCD camera. Drops of diluted dispersions of the helices were deposited on carbon film coated 400-mesh copper grids. Scanning electron microscopy (SEM) was performed with Keyence VE-8800 at 10 kV.

To evaluate the existence of microporous silicon on the entire wall surface of the helical pores, we collected the photoluminescence (PL) from individual helical pores using a confocal fluorescence microscope setup. Optical microscopy was performed in confocal hypersectral and epi-fluorescence modes. For both, the sample was disposed upside down onto a glass coverslip with a small objective oil interlayer (ca.10–20 μm) for index continuity, because of the use of an oil immersion high numerical aperture objective (Olympus UPLSAPO100X0, NA1.40). For the cross-section view, the sample was first cleaved with a “scribe and break” method, and then disposed onto the coverslip taking care of having the cleaved plane parallel to the coverslip by means of a goniometer. The epi illumination source was a 365 nm LED, and a 390 nm long-pass filter was used for the detection on a Hamamatsu ORCA flash4.0 sCMOS camera. The CFM hyperspectral image was acquired with a Picoquant MT200, modified with a Andor Sr303i spectrometer equipped with a Newton EMCCD camera and a home-made software for image reconstruction. The excitation source was a continuous 473 nm laser, and a 490LP filter was used to avoid the detection of the second order diffraction of the excitation light.

3. Results and discussion

Fig. 1a summarizes a series of results for the fabrication of helical nanostructures of polypyrrole. By comparing the cross-sectional views of silicon before and after electropolymerization, complete filling of helical pore with polypyrrole is clearly observed. Helical nanostructures of polypyrrole were successfully obtained after removing the silicon template by immersing the latter in 15 wt% NaOH solution for more than 10 h, clearly replicating the helical pores as observed by TEM. These images clearly show that the structure is not rod-like, but a tube with a constant wall thickness and diameter. It was reported that polypyrrole tended to be deposited as tubes in conventional and non-helical mesoporous and macroporous silicon, whose pore sizes were respectively ~20 nm and ~4 μm and were prepared by anodic dissolution of silicon without metallic catalysts [14]. The results shown in Fig. 1 are therefore in agreement with such previous results.

We then carried out electrochemical filling of the helical pores with gold in view of the numerous new applications of gold nanohelices in nanoelectromechanical systems or plasmonics [17–19]. Fig. 2a summarizes the results on electrochemical gold filling. Cross-sectional observations after electrodeposition shows complete filling of the helical pores as observed for polypyrrole filling. Interestingly, TEM observation of the gold deposits removed from the helical pore template again indicates that they are tubular helices and the inside is empty, similar to the polypyrrole helices shown in Fig. 1d. Although the substrates filled with gold were annealed at 1100 °C, the annealing did not impart a strong effect on the morphology of the gold deposits. Note that electrodeposition of gold was carried out under illumination from the back side of the wafer so that the electrons are effectively supplied to the bottom of the helical pores. However, the gold deposition can also proceed in the dark under a small cathodic current by hole-injection to the valence band. The deposits obtained with and without illumination did not show clear differences, implying that the gold deposits were always tubular.

While the results obtained with polypyrrole were in agreement with our previous studies, those with gold filling were totally unexpected. In order to understand the tubular shape of gold, it is necessary to investigate how the gold deposition on the wall of the helical pores is promoted. The results in Figs. 1 and 2 indicate that the underlying mechanism for the promotion of tubular deposition is the same between anodic and cathodic reactions. Presumably, the determining deposition mechanisms are factors that are not directly related to charge transfer, such as diffusion of the chemicals and their local concentration within the pores. For instance, the accumulation of solutes on the wall surface

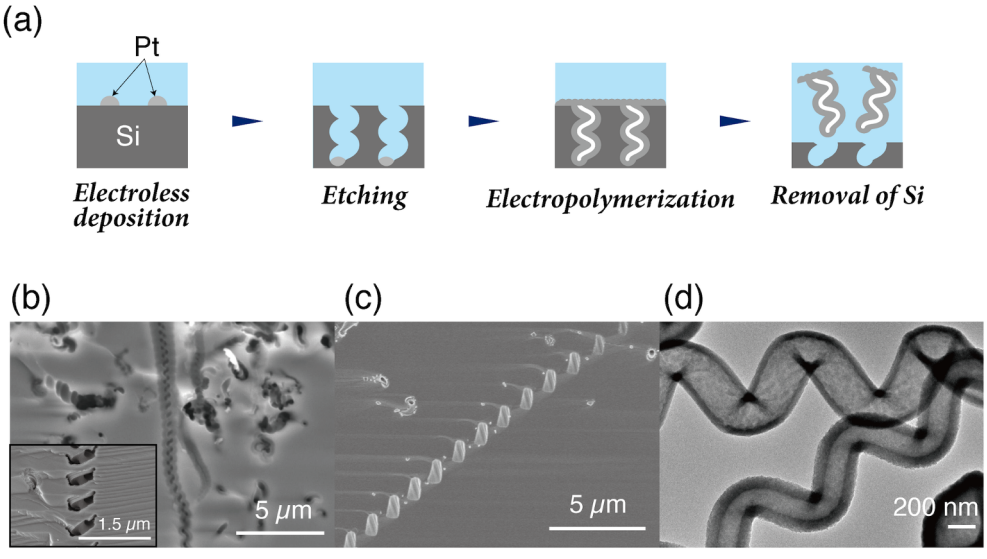

Fig. 1. (a) Schematic illustration of series of experiments for the electrochemical filling of polypyrrole by anodic polymerization. Cross-sectional images before and after the filling are shown in (b) and (c), respectively. The image inserted in (b) is a helical pore typically observed with a high magnification. TEM image of the helical nanostructures of polypyrrole is shown in (d), indicating that the helices are tubes.

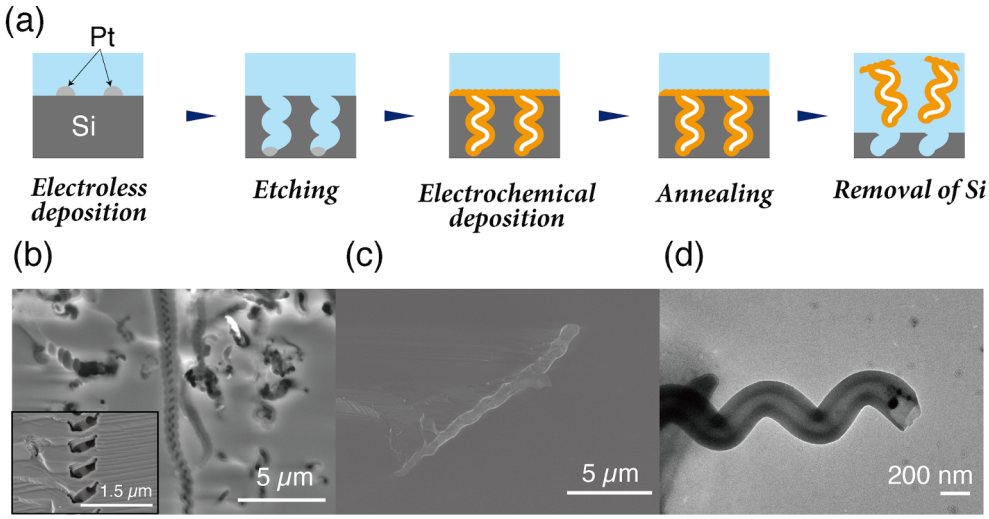

Fig. 2. (a) Schematic illustration of series of experiments for the electrochemical filling of gold by cathodic polymerization. Cross-sectional images before and after the filling are shown in (b) and (c), respectively. The image inserted in (b) is a helical pore typically observed with a high magnification. TEM image of the helical nanostructures of gold is shown in (d), indicating that the helices are tubes as well.

of the helical pores is one of the likely factors that can explain these results. In the previous study, we have clarified that relatively hydrophobic solutes tend to be accumulated within the nanopores of porous silicon [20–23]. When both the pore wall surface and the solute are hydrophobic (solvophobic), surface-induced phase transition within hydrophobic (solvophobic) nanopore is expected to take place and the pores are instantaneously filled with a solution possessing a high concentration of the hydrophobic (solvophobic) solute. Such surface-induced phase transition was observed in electropolymerization of polypyrrole and electrodeposition of metals from their complexes [20,24]. To accumulate within the micropores through surface-induced phase transition, the metal ions must have a low charge density so that their interaction with water is weak, inducing them to behave as relatively hydrophobic metal ions [20]. It should be noted that the surface-induced phase transition within nanopores is more favorable in the case of smaller pores such as microporous silicon whose average pore diameter is ~3 nm [21]. In the case of the helical pores investigated herein, surface-induced phase transitions are not expected considering that the pore size of the helical pores is much larger than conventional micro- and mesoporous silicon. However, our finding that tubular polypyrrole and gold structures were obtained both in anodic electropolymerization and cathodic deposition suggests that the wall surface of the helical pore may be covered with micropores after PacEtch. Actually, the formation of microporous silicon on the wall surface of pores formed by metal-assisted etching of silicon is generally known [25]. Such micropores on the wall surface of the helical pores favors the initial nucleation of polypyrrole and gold due to the accumulation of relatively solvophobic pyrrole and the relatively hydrophobic gold ion complex. The solution for gold deposition used in the present study is known as an alternative solution to toxic cyanide solutions for gold deposition [26]. The electrolyte solution used contains gold complexes with SO_3^{2-} and $S_2O_3^{2-}$ such as $[Au(SO_3)(S_2O_3)]^{3-}$. The ionic size of these gold complexes is quite large with a relatively low charge density, suggesting an overall hydrophobic character. It should be noted that the complex also suppresses the uncontrollable displacement deposition without an external bias. Once the displacement deposition occurs, the deposition takes place mainly at the pore mouths, resulting in the immediate clogging of the pore mouths and in no further deposition inside the pores.

Unfortunately, the pore size of the micropore are ~3 nm, making them difficult to be directly observed by SEM. However, microporous silicon is known to exhibit visible light luminescence at room temperature, suggesting that the presence of micropores can be detected using fluorescence microscopy [27,28]. To test this, we collected the photoluminescence (PL) from the microporous silicon. Fig. 3a shows the PL from the top surface of the silicon substrate after PacEtch observed with a confocal fluorescence microscope, together with the PL spectrum. Unstructured PL emission centered at 610 nm is clearly observed. The latter is attributed to microporous silicon formed on the top surface of the substrate during the PacEtch process. To probe whether the microporous features are also present inside the helical pores, an etched substrate was cleaved and the cross-section was analyzed. Fig. 3b shows the PL from the cross-section of the substrate observed under the same conditions. Although the resolution is limited by diffraction, PL features exhibiting a helical shape are clearly observed. These results indicate that PL originating from microporous silicon is present on the entire surface of the helical pores. Therefore, the formation of helical nanotubes during electrochemical deposition of polypyrrole and gold is likely due to effective nucleation taking place thanks to accumulated solutes in microporous silicon on the wall surface of the helical pores.

To provide additional evidence that microporous silicon accelerates the nucleation on the silicon surface, time traces of the measured potential during the galvanostatic polymerization and deposition were measured. Fig. 4 depicts the variation over time of both anodic electropolymerization and cathodic deposition. In the case of anodic polymerization, the time dependence can be divided into three stages. During Stage-1, the potential gradually increases along with the increase of the overpotential for anodic electropolymerization. Since the deposited polypyrrole film is not highly conductive, the polymerization reaction in Stage-1 takes place on silicon rather than on the deposited polypyrrole. The unpreferable polymerization on the deposited polymer suppresses the increase in thickness of the deposited polymer film. After ca. 15 min, the potential is stabilized as observed in Stage-2. According to this result, Stage-1 corresponds to the preferential deposition of polypyrrole within the microporous silicon existing on the wall surface of the helical pores, and then at Stage 2 the silicon wall is totally covered with polypyrrole. In the transient period from Stage-2 to Stage-3, the pore mouth (where deposition is expected to be favored due to mass transport) is closed, and no further polymerization can occur inside the helical pores. It is then expected that film growth occurs on the top surface of the substrate during Stage-3. With increasing polymerization time, the thickness of the film increases. This increase results in the increase of resistance of the polypyrrole film, and thus the stepwise increases in overpotential is observed in electropolymerization. The filling process is summarized as shown in Fig. 4c.

The temporal behavior for gold deposition is significantly different compared to electropolymerization since gold is highly conductive. Still, the deposition kinetics can again be divided into three stages. In Stage-1, accelerated deposition of gold within the microporous silicon is

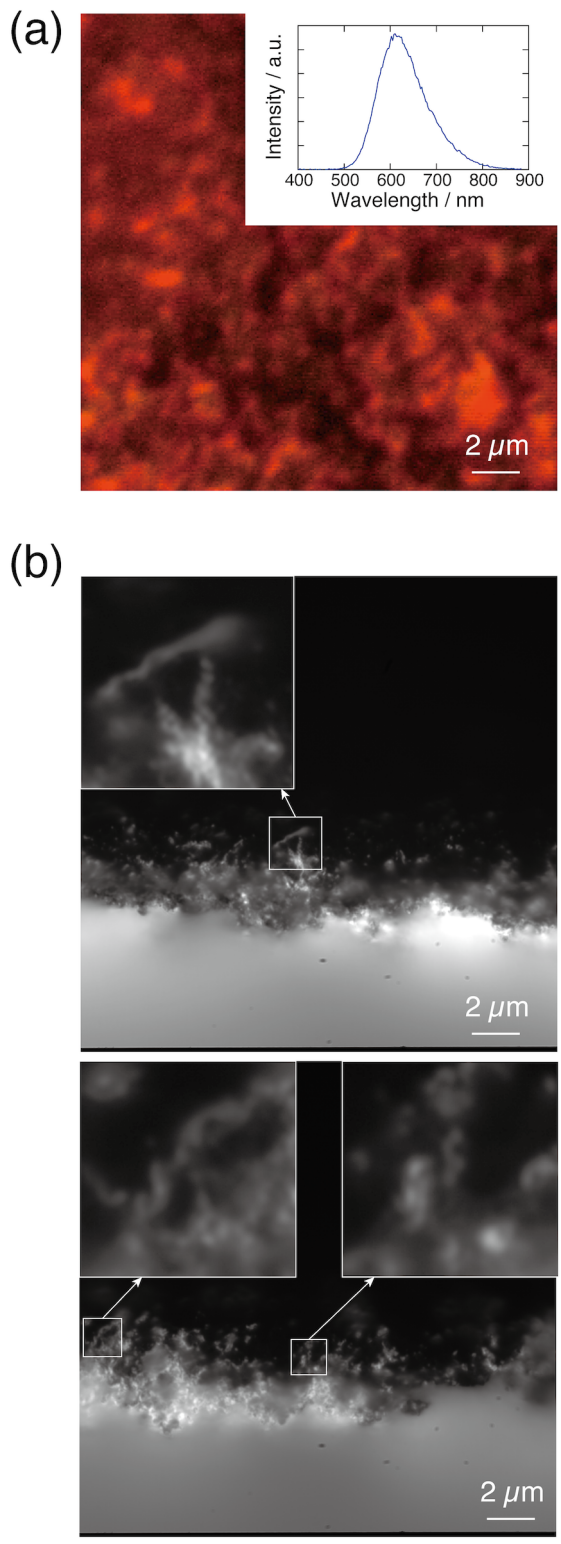

Fig. 3. (a) Photoluminescence from the top surface of the silicon substrate after PacEtch, together with the spectrum of the luminescence. Images in (b) show the photoluminescence from the cross-section observed using a microscope. In the magnified images, luminescence shows helical shapes, suggesting that microporous silicon remains on the wall surface of the helical pores.

expected as reported in our previous study on platinum electrodeposition [21]. Since the deposition of gold within the microporous silicon is fast, the gold ions are gradually depleted within the pores. Therefore, the potential shifts to negative values to increase the deposition rate and maintain a constant current density. Once the deposition within the microporous silicon is finished, the ensuing deposition process begins to increase the thickness of the gold nanotubes and the potential slowly returns to less negative values since the availability of the gold ions is expected to be greater within the helical pores due to their much larger diameter compared to the micropores. This process corresponds to Stage-2 and results in the increase of the thickness of the gold tube walls. Since the ionic transport from the bulk solution to the top surface of the substrate is relatively high, the overpotential must decrease when the helical pore is filled and the deposition starts on the top surface, as measured in Stage-3. In the case of electrodeposition, the deposition rate is proportional to the concentration of metallic ions in the vicinity of the wall surface as well as to the reaction rate constant which is a function of the overpotential. Even if the overpotential is high enough to promote the electrodeposition, the deposition rate can be slow when the concentration of metallic ions in the vicinity of the wall surface is low. Since the metallic ions are supplied from the bulk solution, the pore mouths are the most favored in view of the concentration of the metallic ions. This means that the deposition rate at the pore mouths is faster than the inside of the helical pores, leading to the clogging of the pore mouths before the complete filling of the helical pores. Thus, in both polypyrrole and gold deposition, Stage-1 corresponds to the filling of microporous silicon on the entire surface of the walls of the helical pores. In contrast to helical pores formed by PacEtch, conventional meso- and macroporous silicon formed by anodization without metallic catalysts are not covered with microporous silicon. For this reason, the Stage-1 behavior shown in Fig. 4 was not previously observed in the electrodeposition of conventional meso- and macroporous silicon that is formed by anodization without metallic catalysts, therefore yielding rod-like deposits without any voids. Note that the thickness of the tubes can be controlled if one controls the time for deposition within Stage-2. However, the thickness shown in Figs. 1 and 2 were the maxima due to the clogging of the pore mouths. Theoretically speaking, the thickness can be controlled below the maxima.

In view of applications of the helices fabricated in the present study, the tubular nature of the material may be important for some applications. In the case of plasmonic applications, the excitation of plasmon polaritons is generally localized on the metal surface irradiated by the incident electromagnetic wave and the presence or absence of void may have a significant effect depending on the thickness of the wall that is deposited. On the other hand, for applications for chiral chemistry, we note that the chiral information is contained on the outside surface of the helical tubes, but that the interior also possesses a chiral helical morphology. Therefore, the accessibility of the inside volume may affect the overall chiral induction of the material.

The fabrication of completely filled metallic helical tubes may be possible using techniques similar to the copper deposition for the fabrication of integrated circuts. In this system, effective additives in the electrolyte solutions were used, generally termed accelerator and inhibitor in the case of copper deposition. Thanks to the use of additives in solution, copper can be deposited without any voids.

4. Conclusions

Electrochemical filling of helical pores produced by PacEtch of silicon is a promising strategy to fabricate conductive helical nanotubes. In the present study, we focused on understanding the origin of a possible common mechanism for anodic polymerization and cathodic deposition. We concluded that microporous silicon is formed on the wall surfaces of the helical pores after PacEtch, and that this enhances uniform nucleation on the wall to favor the growth of helical nanotubes. The enhancement of the nucleation is explained in the framework of our previous study, i.e., surface-induced phase transition within the nanopores. We believe that the present study gives a new insight that electrochemistry can play a role for the production of chiral helical nanostructures without the use of chiral molecules.

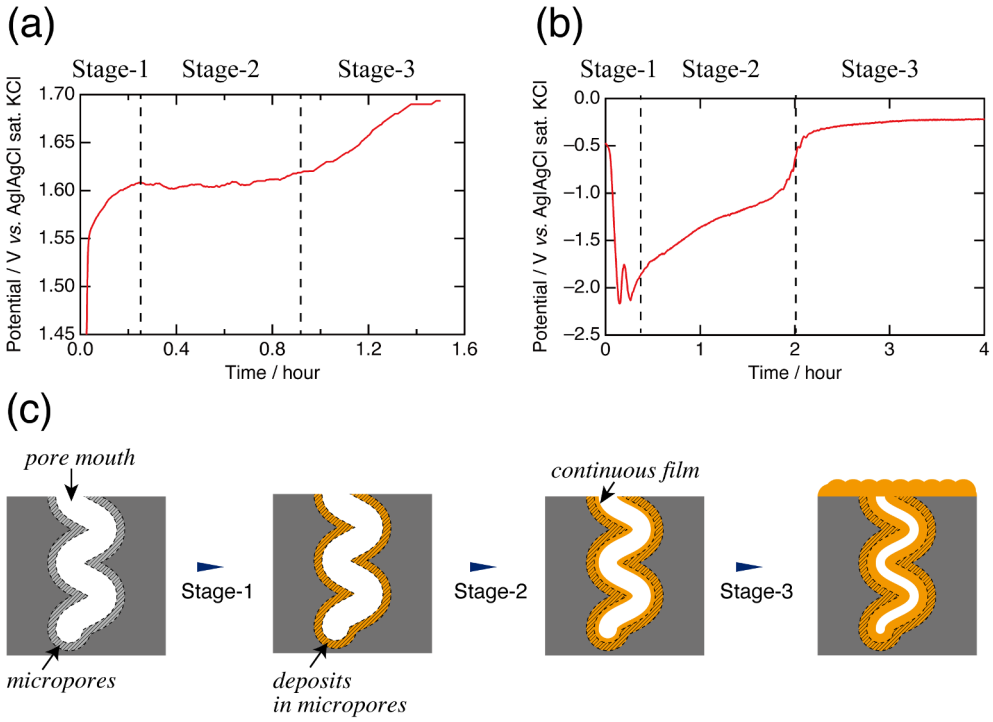

Fig. 4. Time developments of potential during the electrochemical filling. Plot in (a) and (b) were obtained during the anodic polymerization and cathodic deposition, respectively. Both of the time developments are commonly divided into three stages. Illustrations in (c) details the process at each stage.

CRediT authorship contribution statement

Yuki Maeda: Methodology, Investigation, Validation, Writing - original draft. **Takumi Yasuda:** Investigation, Validation, Writing - review & editing. **Kenta Matsuzaki:** Methodology, Investigation, Validation. **Yutaka Okazaki:** Validation, Writing - review & editing. **Emilie Pouget:** Investigation, Validation, Writing - review & editing. **Reiko Oda:** Validation, Writing - review & editing, Funding acquisition. **Atsushi Kitada:** Validation, Writing - review & editing. **Kuniaki Murase:** Validation, Writing - review & editing. **Guillaume Raffy:** Investigation, Validation. **Dario M. Bassani:** Investigation, Validation, Writing - review & editing. **Kazuhiro Fukami:** Conceptualization, Methodology, Writing - original draft, Supervision, Project administration, Funding acquisition.

Acknowledgments

This work was supported by The Kyoto University Foundation, Japan, by the Supporting Program for Interaction-Based Initiative Team Studies (Kyoto University), and partly by Kyoto University Nano Technology Hub in “Nanotechnology Platform Project” sponsored by the Ministry of Education, Culture, Sports, Science and Technology (MEXT), Japan. This work was also supported by the Centre National de la Recherche Scientifique and the University of Bordeaux through the France-Japan International Associated Laboratory on Chiral Nanostructures for Photonic Applications (LIA-CNPA).

References

[1] T. Yamamoto, Y. Akai, M. Suginome, Chiral palladacycle catalysts generated on a single-handed helical polymer skeleton for asymmetric arylative ring opening of 1,4-Epoxy-1,4-dihydronaphthalene, Angew. Chem. Int. Ed. 53 (2014) 12785–12788.
[2] M. Matuschek, D.P. Singh, H.-H. Jeong, M. Nesterov, T. Weiss, P. Fischer, F. Neubrech, N. Liu, Chiral plasmonic hydrogen sensors, Small 14 (2018) 1702990.
[3] H.-H. Jeong, A.G. Mark, P. Fischer, Magnesium plasmonics for UV applications and chiral sensing, Chem. Commun. 52 (2016) 12179–12182.
[4] D. Kosters, A. De Hoogh, H. Zeijlemaker, H. Acar, N. Rotenberg, L. Kuipers, Core-shell plasmonic nanohelices, ACS Photonics 4 (2017) 1858–1863.
[5] J.K. Gansel, M. Thiel, M.S. Rill, M. Decker, K. Bade, V. Saile, G. Von Freymann, S. Linden, M. Wegener, Gold helix photonic metamaterial as broadband circular polarizer, Science 325 (2009) 1513–1515.
[6] Y. Shang, X. He, Y. Li, L. Zhang, Z. Li, C. Ji, E. Shi, P. Li, K. Zhu, Q. Peng, C. Wang, X. Zhang, R. Wang, J. Wei, K. Wang, H. Zhu, D. Wu, A. Cao, Super-stretchable spring-like carbon nanotube ropes, Adv. Mater. 24 (2012) 2896–2900.
[7] E. Yashima, N. Ousaka, D. Taura, K. Shimomura, T. Ikai, K. Maeda, Supramolecular helical systems: helical assemblies of small molecules, foldamers, and polymers with chiral amplification and their functions, Chem. Rev. 116 (2016) 13752–13990.
[8] M.V. Kelso, J.Z. Tubbesing, Q. Chen, J.A. Switzer, Epitaxial electrodeposition of chiral metal surfaces on silicon(643), J. Am. Chem. Soc. 140 (2018) 15812–15819.
[9] C. Wattanakit, T. Yutthalekha, S. Asssavapanumat, V. Lapeyre, A. Kuhn, Pulsed electroconversion for highly selective enantiomer synthesis, Nat. Commun. 8 (2017) 2087.
[10] S. Assavapanumat, M. Ketkaew, A. Kuhn, C. Wattanakit, Synthesis, Characterization, and electrochemical applications of chiral imprinted mesoporous Ni surfaces, J. Am. Chem. Soc. 141 (2019) 18870–18876.
[11] K. Tsujino, M. Matsumura, Helical nanoholes bored in silicon by wet chemical etching using platinum nanoparticles as catalyst, Electrochem. Solid State Lett. 8 (2005) C193–C195.
[12] T. Yasuda, Y. Maeda, K. Matsuzaki, Y. Okazaki, R. Oda, A. Kitada, K. Murase, K. Fukami, Spontaneous symmetry breaking of nanoscale spatiotemporal pattern as the origin of helical nanopore etching in silicon, ACS Appl. Mater. Interfaces 11 (2019) 48604–48611.
[13] K. Fukami, F.A. Harraz, T. Yamauchi, T. Sakka, Y.H. Ogata, Fine-tuning in size and surface morphology of rod-shaped polypyrrole using porous silicon as template, Electrochem. Commun. 10 (2008) 56–60.
[14] K. Fukami, M.L. Chourou, R. Miyagawa, Á.M. Noval, T. Sakka, M. Manso-Silván, R.J. Martín-Palma, Y.H. Ogata, Gold nanostructures for surface-enhanced Raman spectroscopy, prepared by electrodeposition in porous silicon, Materials 4 (2010) 791–800.
[15] K. Rumpf, P. Granitzer, N. Koshida, P. Poelt, H. Michor, Morphology controlled magnetic interactions in metal embedded porous silicon nanostructures, ECS J. Solid State Sci. Technol. 4 (2015) N41–N43.
[16] T. Kim, X. Fu, D. Warther, M.J. Sailor, Size-controlled Pd nanoparticle catalysts prepared by galvanic displacement into a porous Si-iron oxide nanoparticle host, ACS Nano 11 (2017) 2773–2784.
[17] J.R. Dunklin, G.T. Forcherio, K.R. Berry, D.K. Roper, Asymmetric reduction of gold nanoparticles into thermoplasmonic polydimethylsiloxane thin films, ACS Appl. Mater. Interfaces 5 (2013) 8457–8466.
[18] H. Schlicke, D. Battista, S. Kunze, C.J. Schröter, M. Eich, T. Vossmeyer, Freestanding membranes of cross-linked gold nanoparticles: novel functional materials for electrostatic actuators, ACS Appl. Mater. Interfaces 7 (2015) 15123–15128.
[19] R.G. Freeman, K.C. Grabar, K.J. Allison, R.M. Bright, J.A. Davis, A.P. Guthrie, M.B. Hommer, M.A. Jackson, P.C. Smith, D.G. Walter, M.J. Natan, Self-assembled

metal colloid monolayers: an approach to SERS substrates, Science 267 (1995) 1629–1632.
[20] K. Fukami, R. Koda, T. Sakka, Y. Ogata, M. Kinoshita, Electrochemical deposition of platinum within nanopores on silicon: drastic acceleration originating from surface-induced phase transition, J. Chem. Phys. 138 (2013) 094702.
[21] A. Koyama, K. Fukami, T. Sakka, T. Abe, A. Kitada, K. Murase, M. Kinoshita, Penetration of platinum complex anions into porous silicon: anomalous behavior caused by surface-induced phase transition, J. Phys. Chem. C 119 (2015) 19105–19116.
[22] A. Koyama, K. Fukami, Y. Suzuki, A. Kitada, T. Sakka, T. Abe, K. Murase, M. Kinoshita, High-rate charging of zinc anodes achieved by tuning hydration properties of zinc complexes in water confined within nanopores, J. Phys. Chem. C 120 (2016) 24112–24120.
[23] A. Koyama, K. Fukami, Y. Imaoka, A. Kitada, T. Sakka, T. Abe, K. Murase, M. Kinoshita, Dynamic manipulation of local pH within nanopore triggered by surface-induced phase transition, Phys. Chem. Chem. Phys. 19 (2017) 16323–16328.
[24] A. Koyama, K. Fukami, T. Yamauchi, N. Nishi, T. Sakka, A. Kitada, K. Murase, Lateral growth of polypyrrole electropolymerized along hydrophobic insulative substrates, ECS Electrochem. Lett. 3 (2014) G5–G7.
[25] C. Chartier, S. Bastide, C. Lévy-Clément, Metal-assisted chemical etching of silicon in HF-H_2O_2, Electrochim. Acta 53 (2008) 5509–5516.
[26] T. Osaka, A. Kodera, T. Misato, T. Homma, Y. Okinaka, O. Yoshioka, Electrodeposition of soft gold from a thiosulfate-sulfite bath for electronics applications, J. Electrochem. Soc. 144 (1997) 3462–3469.
[27] A.G. Cullis, L.T. Canham, P.D.J. Calcott, The structural and luminescence properties of porous silicon, J. Appl. Phys. 82 (1997) 909–965.
[28] M.V. Wolkin, J. Jorne, P.M. Fauchet, G. Allan, C. Delerue, Electronic states and luminescence in porous silicon quantum dots: the role of oxygen, Phys. Rev. Lett. 82 (1999) 197–200.